Review

Abrasion evaluation of Moon and Mars simulants on rotating shaft/sealing materials: simulants and structural materials review and selection

György Barkó[1], Gábor Kalácska[1], Róbert Keresztes[1], Zsidai László[1], Hailemariam Shegawu[1] and Ádám Kalácska[2]*

[1] Institute of Technology, Szent István Campus, MATE, Páter Károly u. 1, 2100 Gödöllő, Hungary; barko.gyorgy.csaba@uni-mate.hu

[2] Soete Laboratory, Department of Electromechanical, Systems and Metal Engineering, Ghent University, Technologiepark 46, B-9052, Zwijnaarde, Belgium;

* Correspondence: adam.kalacska@ugent.be

Abstract: Tribological testing of moving shaft/sealing pairs in complex environments is at the front-line of research. Machines working in abrasive conditions are subject to different wear effects. It is valid not only on the Earth but especially valid for rovers and future robots used in Mars and Moon missions. The aim of our joint research with the European Space Agency is to study the abrasion phenomena of moving machine elements on Mars and the Moon, by using artificial soil samples ("simulants"). This review detail the available simulant sources and recommend a selection of the most suitable ones for tribological testing. Moreover, the potential mating structural materials subjected to abrasive space applications are reviewed. The tribological tests are exploring the features of the rotary shaft/seal relationship that is subject to dry friction and intense abrasion. By using the simulants, measurements are performed under laboratory conditions with both a sample test and a real shaft/seal connection. Parameters of the selection criteria have been defined and classification of the simulant sources were made. It was found that simulant particle size distribution and chemical substance content is detailed enough only for a limited type of available artificial Moon and Mars soil samples. 4 simulants have been identified and applied later in the tribological testing. For the shaft materials, based on a detailed case study of polymers, steel and aluminium alloys, a high-strength aluminium alloy with a hard anodized surface and a stainless steel were selected for further abrasion tests.

Keywords: mars simulant; moon simulant; rotary shaft; sealings

1. Introduction

Application of regolith simulants in test laboratories is general practice [1]. These artificial regolith samples prepared, are similar to those found on planetary surfaces. Thanks to the lander and rover missions sent to explore Mars, details are available on the substance composition of the soil at different sites across the planet. Two of the earliest Martian missions, the Viking I and II landers, scrape away at the top few centimetres of the regolith surrounding the landing sites (Table 1).

Preprints (www.preprints.org) | NOT PEER-REVIEWED | Posted: 15 June 2023 doi:10.20944/preprints202306.1135.v1

Table 1. Constitution of Mars Surface Soil [2].

Parameters	Viking Lander I – Surface Soil (%)
SIO_2	43
FeO	0
Fe_2O_3	18.5
Al_2O_3	7.3
SO_3	6.6
MgO	6.0
CaO	5.9

Mars mission 'Pathfinder' successfully landed on the Martian surface in 1997, deploying the Sojourner rover. This mission demonstrated the feasibility of traversing the Martian regolith and provided additional information about it. Sojourner also performed the wheel abrasion experiment (WAE) and utilized it to profile the abrasiveness of the regolith particles and give information about the shapes of the particles. Subsequently, the MER missions utilised the first optical microscopes on Mars. Rovers were equipped also with spectrometers providing real composition data from a huge range of sites. Lander mission to Mars, InSight and Phoenix, extended the results originating from the Viking missions. The thermal and evolved gas analyzer (TEGA) on the landers profiled the substances in the regolith further. Also, the trenches left by the rover scoop action provided information about the mechanical properties of the soil.

There is a renewed interest in exploring the Moon, leading to upcoming missions by various space agencies, including the U.S., Russia, China, Japan, the EU, and Canada [3]. Lunar regolith simulant is required to develop rover missions that can successfully explore the surface of the Moon. These regolith simulants shall accurately represent the soils that exist on the Moon's surface. Several high-fidelity simulants are available based on chemical substance content, particle size distribution and particle shape. These artificial regolith products are offered to test different applications. Simple simulants used the fine fraction of grinded granular basalts with surface weathering. Advanced simulants utilized state-of-the-art technology to approach closely the original regolith composition and substance content/ratio as well as the electrostatic behaviour.

Newson et al. [3] characterized the geomechanical performance of various simulants. The outcomes of the mechanical property tests revealed that the simulants exhibit comparable mechanical responses to angular and rough soils and their behaviour aligns closely with that of two widely recognized geotechnical benchmark soils, establishing their reliability and applicability in geotechnical studies.

Preparation of Moon or Mars soil simulants and selecting raw materials for artificial regolith is challenging. The experimental process shall ensure the Earth-based raw materials used in these processes are comparable in their physical and mechanical properties to those observed on the Moon or Mars. Specifications for internal friction angle and cohesion can be utilized as general mechanical parameters. Particle size distribution, dry bulk density and particle shape must be considered as well. For geomechanical testing, high fidelity of chemical substance content/ratio is not a priority for the selection of simulants.

This paper provides a collection of potential Mars and Moon simulants, compare them based on chemical composition and size distribution, and provide recommendation for the selection of the most suitable simulants for tribological testing. Also, the commonly used shaft and sealing materials subjected to abrasive conditions in space are analyzed and reviewed.

2. Materials

2.1. Review on the preparation of Martian and Lunar abrasive simulants

Martian simulants have been prepared by Böttger et al [4]. Simulants were used to specifically test the Raman Laser Spectrometer (RLS) on the ExoMars rover and its ability to identify organics

Preprints (www.preprints.org) | NOT PEER-REVIEWED | Posted: 15 June 2023 doi:10.20944/preprints202306.1135.v1

and minerals. They were meant to represent the environmental change on Mars from early hydrothermal alteration to later cold and dry oxidizing conditions. The materials were crushed and mixed, then sieved to a <1 mm size fraction for experiments. The components are described in Table 2.

Table 2. Mineralogical composition of Phyllosilicatic Mars Regolith Simulant (P-MRS) and Sulfatic Mars Regolith Simulant (S-MRS) [4].

Component	P-MRS (wt.%)	S-MRS (Wt.%)
Gabbro	3	32
Olivine	2	15
Quartz	10	3
Hematite	5	13
Montmorillonite	45	-
Charmosite	20	-
Kaolinite	5	-
Siderite	5	
Hydromagnesite	5	-
Goethite	-	7
Gypsum	-	30

A specific simulant "JSC" has been developed by Allen et al [5]. JSC Mars-1 has been prepared for scientific research as well as for engineering tests and academic purposes. JSC Mars-1 is the <1 mm fraction of weathered volcanic ash from Pu'u Nene, which is a residue of the cone on the Island of Hawaii. Pu'u Nene ash has also been selected based on its spectral similarity to material located on bright regions of Mars. This kind of simulant is available in significant quantity. Chemical composition compared to Viking landers (VL-1 and VL-2) and Pathfinder composition data (Table 3) and grain size distribution are shown in Table 4.

Table 3. Pathfinder data about chemical composition [5].

	VL-1	WL-2	Pathfinder	JSC Mars-1	
Oxide	Wt%*	Wt%*	Wt%**	Wt%***	Wt%****
SiO_2	43	43	44.0	34.5	43.5
Al_2O_3	7.3	7	7.5	18.5	23.3
TiO_2	0.66	0.56	1.1	3.0	3.8
Fe_2O_3	18.5	17.8	16.5	12.4	15.6
MnO	n.a.	n.a.	n.a.	0.2	0.3
C_aO	5.9	5.7	5.6	4.9	6.2
MgO	6	6	7.0	2.7	3.4
K_2O	<0.15	<0.15	0.3	0.5	0.6
Na_2O	n.a.	n.a.	2.1	1.9	2.4
P_2O_5	n.a.	n.a.	n.a.	0.7	0.9
SO_3	6.6	8.1	4.9	n.a.	n.a.
Cl	0.7	0.5	0.5	n.a.	n.a.
LOI	n.a.	n.a.	n.a.	21.8	n.a.
Total	89	89	89.5	101.1	100.0

 doi:10.20944/preprints202306.1135.v1

Table 4. Grain size distribution [5].

Size (μm)	Wt%
1000-450	21
449-250	30
249-150	24
149-53	19
52-5	5
< 5	1

Another widely used simulant was developed by Cannon et al [6]. The paper describes the Mars Global Simulant (MGS-1), a high-fidelity mineralogical representative of basaltic regolith on Mars. The prototype simulant was utilized to characterize basic physical, chemical and spectral properties as well as volatile content. MGS-1 simulant has been applied to test Mars rovers and remote sensing equipment. This kind of simulant is produced in large amounts by the Center for Lunar & Asteroid Surface Science (CLASS) Exolith Lab and it is commercially available. By publishing the mineral recipe and production methods, authors anticipate that other groups can recreate the simulant and modify it as they see fit, leading to a more sustainable model for simulant production and the possibility of extending the simulant for different regions on Mars or different applications.

An analogue approach has been used by Exolith Lab to prepare the Jezero crater simulant. Jezero Delta Simulant (JEZ-1) was made to simulate materials in the Jezero Crater deltas. This is the geographical area that is investigated by the NASA Mars 2020 rover mission. Based on orbital remote sensing of Jezero delta deposits, JEZ-1 is a mixture of MGS-1 composition with smectite clay, magnesium carbonate, and olivine. Due to potential mineralogical deviations, limitations in simulant fidelity must be considered.

Soil sample extraction tests, excavation or rover mobility evaluation require a significant amount of simulant up to a couple of hundred kilograms. High-fidelity simulants are expensive and not available in such order of magnitude to fill in the rover test bed. Low-fidelity simulants have been proven to be a reasonable trade-off and applicable to these tests. However, test results must be carefully calculated and geotechnical properties to be reported in detail, allowing to repeat the experiments in a relevant test environment. This process step is missed in several excavation studies reported.

Low fidelity but large-scale Lunar simulant has been made and evaluated by Just et al [7]. Large-scale engineering experiments involving excavation, sampling, and mobility in rocky planetary surface exploration, such as on the Moon, frequently demand extensive test beds filled with significant quantities of soil, often amounting to hundreds of kilograms. However, specially engineered regolith simulants are expensive and may not be available in sufficient quantities due to limited production rates. As a result, the use of low-fidelity analogues becomes a practical alternative. Nevertheless, it is crucial to report the geotechnical properties of these analogues to accurately calculate excavation and traction forces, and ensure comparability and repeatability of results. Unfortunately, this vital step of characterizing the analogues is often overlooked in studies focusing on regolith handling and excavation.

Two low-fidelity simulants, UoM-B and UoM-W, have been identified as potential candidates for large-scale simulant testbed experiments. Both geotechnical characteristics (particle morphology, particle size distribution, specific gravity, maximum and minimum densities, and shear strength parameters) and chemical substance content have been investigated. Results acquired have been relevant to values of other available Moon regolith simulants, as well as features of Apollo regolith samples. However, the chemical content of UoM-B and UoM-W are different from the Moon regolith obtained during Apollo missions, both simulants demonstrated meaningful similarity from a mechanical property standpoint that allows us to apply them for low-fidelity but large-scale experiments. Linke et al [8] dedicated efforts to develop Lunar Mare and Lunar Highland simulants. The TUBS-M = Mare; TUBS-T = Highlands simulants originated from basaltic and anorthositic bedrock. The aim was to match the two dominant lunar surface rock types. In terms of raw material sources, TUBS-M has been prepared from an alkali-olivine basalt in Germany. The material to manufacture TUBS-T originated from a Scandinavian metamorphosed gabbroic complex. The production process

Preprints (www.preprints.org) | NOT PEER-REVIEWED | Posted: 15 June 2023 doi:10.20944/preprints202306.1135.v1

of the two simulants has been described. Their characteristics in terms of mineralogy (Table 5), chemical composition (Table 6), and physical properties (Table 7) are presented:

Table 5. Mineralogy [8].

Component	TUBS-M (wt.%)	TUBS-T (wt.%)
Basalt	100	0
Anorthosite	0	100

Table 6. Bulk chemistry [8].

Oxide	TUBS-M (wt.%)	TUBS-T (wt.%)
SiO_2	48.61	48.71
TiO_2	2.29	0.12
Al_2O_3	13.28	30.33
FeO>	10.14	1.05
MgO	8.73	0.57
CaO	8.31	14.57
Na_2O	3.67	3.05
K_2O	1.71	0.22
MnO	0.18	0.015
Cr_2O_3	0.04	0.00

Table 7. Physical properties [8].

Property	TUBS-M	TUBS-T
Grain density	2.96 g/cm³	2.71 g/cm³
Bulk density	1.41 g/cm³	1.18 g/cm³
Angle of repose	41.9 – 45.8°	37.91°
Particle size range	0 – 2.0 mm	0 – 2.0 mm
Median	87 µm	87 µm
Cohesion	0.6 kPa	1.46 kPa

Figure 1. TUBS-M and TUBS-T lunar regolith simulants.

A wide range of large amounts of Lunar simulants and additives are offered by the enterprise Off Planet Research [9]. Two major simulants offered are Archean Anorthosite (Source: Shawmere Anorthosite Complex, Foleyet, Ontario, Canada) and Basaltic Cinder (Source: San Francisco Formation in Arizona, USA). Archean Anorthosite is mineralogically similar to the Lunar mineral form. Anorthosite originated from Canada was primary feedstock source preparing Lunar Highland simulants. Anorthosites from this source have been proven to be unaltered from the original state. Basaltic Cinder from Arizona is mineralogically comparable to Lunar Mare low-titanium basalt regolith and has high glass content which supports its use as a simulant for basaltic regolith. Several added components are offered as well, including material: Ilmenite (titanium and iron-based mineral,

Preprints (www.preprints.org) | NOT PEER-REVIEWED | Posted: 15 June 2023 doi:10.20944/preprints202306.1135.v1

standard concentration = 14.4%), Agglutinates, Iron and Iron dioxide, and Silica dioxide. The company offer several customized mixtures made from the materials above. The LMS-1 Lunar Mare Simulant has been developed by the CLASS Exolith Lab [10]. It is a high-fidelity, mineral-based simulant appropriate for a generic or average mare location on the Moon. The simulant is not made of a single terrestrial lithology but accurately captures the texture of lunar regolith by combining both mineral and rock fragments (i.e., polymineralic grains) in accurate proportions. The particle size distribution of the simulant is targeted to match that of typical Apollo soils. Physical Properties are summarized below.

- Mean Particle Size: 50 μm
- Median Particle Size: 45 μm
- Particle Size Range: <0.04 μm – 300 μm
- Uncompressed Bulk Density: 1.56 g/cm^3

At present, LMS-1 does not replicate the characteristics of agglutinates or nanophase iron in its composition. The mineralogical table (Table 8) summarizes the properties below:

Table 8. Components of LMS-1 [10].

Component	Wt. %
Pyroxene	32.8
Glass-rich basalt	32.0
Anorthosite	19.8
Olivine	11.1
Ilmenite	4.3

The table (Table 9) originated from CLASS Exolith Lab below shows the relative abundances of each element detected by X-ray fluorescence (XRF).

Table 9. Oxides [10].

Oxide	Wt. %
SiO_2	46.9
TiO_2	3.6
Al_2O_3	12.4
FeO	8.6
MnO	0.6
MgO	16.8
CaO	7.0
Na_2O	1.7
K_2O	0.7
P_2O_5	0.2

LMS-1 contain these chemical elements as minerals described in Table 8 and not necessarily in oxide form as listed in Table 9. Artificial regolith GREENSPAR origin is Greenland Anorthosite provided by Hudson Resources, Inc. [11] located 85 km southwest of Kangerlussuaq, Greenland. This Anorthosite has 90% Plagioclase Feldspar, and evolved in a low quartz environment, resulting in less than 10% being other minerals. Lunar highlands are dominated by plagioclase feldspar. The GREENSPAR product is available in different size ranges, e.g. GreenSpar 250 (≤ 250μm) and GreenSpar 90 (≤ 90μm) [11]. NASA Johnson Space Center's ARES division has evaluated the use of GREENSPAR 250 for potential use as a component of lunar highlands as well as polar regolith simulants. Table 10 lists the oxides in this simulant.

Preprints (www.preprints.org) | NOT PEER-REVIEWED | Posted: 15 June 2023 doi:10.20944/preprints202306.1135.v1

Table 10. Major oxides of GreenSpar [11].

Major oxides	Average Weight %
SiO_2	50.18
Al_2O_3	30.88
Fe_2O_3	0.49
MgO	0.19
CaO	14.58
Na_2O	2.63
K_2O	0.23
TiO_2	0.05
P_2O_5	0.01
MnO	<0.01
Cr_2O_3	<0.01
V_2O_5	<0.01

Anorthosite is a significant constituent of the lunar crust and plays a crucial role, potentially even a predominant one, in the composition of the lunar regolith. Battler et al [12] performed research to prepare a simulant with grain size distribution similar to Apollo 16 sample 64 500. Earth-based anorthosite has been selected as raw material and several crushing experiments made. Basic simulant originated from granoblastic facies of the Archean Shawmere Complex of the Kapuskasing Structural Zone of Ontario, Canada. This base simulant had minimal retrogression and was found to be homogeneous and characteristic of Lunar Highland. Extensive quarry operations have been performed due to previous industrial interest in this anorthosite. The availability of this simulant in large amounts is an advantage due to the simple access and extraction of its raw material.

Another simulant based on Shawmere, OB-1 has additional olivine content. This simulant is manufactured by Deltion Innovations to replicate the lunar highlands regolith It has been crushed to achieve the particle size distribution with glass components of the Apollo 16 sample mentioned above. These simulants are available on a large scale to test drilling and excavation operations as well as evaluate construction options for future Moon projects. Table 11 and Table 12 summarize the key properties of OB1:

Table 11. Physical properties of OB-1 simulant [12].

Property	Value
Mean particle size	82.25 μm
Median particle size	35.97 μm
Specific gravity	3.071
Bulk density	1.815 g/cm^3

 doi:10.20944/preprints202306.1135.v1

Table 12. Major element chemistry of OB-1 simulant [12].

Oxide	Apollo 16 Average Soil wt. %	OB-1	Shawmere Anorthosite Avg. wt %
SiO_2	45	-	48.28
Al_2O_3	26.7	-	32.01
FeO	-	-	1.34
Fe_2O_3	-	-	0.09
MgO	6.14	-	0.22
CaO	15.3	-	15.43
Na_2O	0.457	-	2.38
K_2O	0.12	-	0.16
TiO_2	0.595	-	0.05
P_2O_5	-	-	0.01
MnO	-	-	0.01
Cr_2O_3	-	-	-
V_2O_5	-	-	-

2.2. Frequently applied materials for space application subjected to possible abrasive conditions

2.2.1. Requirement for target materials

Scopus, Web of Knowledge and Google Scholar have a wealth of published articles on the conditions and characterisation of space. A common feature is that, in addition to vacuum and other pressure conditions, radiation and temperature conditions, as well as local weather conditions, play a prominent role. A number of papers describe the characterisation and expected effects of dust storms in Martian conditions.

Based on three authoritative review summaries [13]–[15] and some specific articles [16]–[22], the impacts on structural materials and their characteristics can be summarised as follows. As it is concluded in [14] outer space encompasses various unique environments and forces that differ significantly from those experienced on Earth. These include high-energy charged particles, ultraviolet (UV) radiation, meteoroids, and orbital debris [16]. These factors can have detrimental effects on the behaviour of construction materials and can alter fundamental aspects of loading and mechanics. Essentially, there are three key distinctions between the environments of Earth, the Moon, and Mars. These differences pose critical challenges and are commonly classified as 1) absence of atmosphere; 2) extreme radiation; 3) variations in gravity. Earth's atmosphere consists of a specific gas composition, primarily Oxygen (21%) and Nitrogen (78%), with traces of Carbon Dioxide, Neon, and others. The Moon is considerably smaller with correspondingly lower gravity and technically lacks an atmosphere. Mars possesses an atmosphere about 100 times thinner than the Earth and mainly consists of Carbon Dioxide, Nitrogen and Argon [17]. The Moon and Mars share the characteristic of having a very thin atmosphere, which offers limited protection against meteorites and micrometeorites. Lindsey [18] highlighted that micrometeorites can reach velocities of 20–70 km/s. Toutanji et al. [19] examined the impact of similar particles, firing projectiles weighing 1.4 x 10-4 g into concrete specimens at a speed of 5.9 km/s. The result was the formation of craters with diameters of 13 mm. These experiments, along with the investigations conducted by Nealy et al. [20], underscore the destructive nature of meteorite impacts, the necessity for effective protection against larger meteorites, and the importance of durable and resilient construction materials. Due to the absence of an atmosphere, temperature fluctuations and low pressure are prevalent. On the Moon, the temperature shifts between -173 and 127 ℃, while it remains intensely cold on Mars at about -57 ℃. The adverse effects of vacuum are magnified with the absence of the atmosphere. In comparison, the vacuum of space varies from 3 x 10-13 kPa on the Moon to 0.7 kPa on Mars (in contrast to 101.3 kPa on Earth). Under vacuum conditions, materials can experience outgassing, releasing volatile substances. Kanamori et al. [21] investigated the long-term exposure of mortar to vacuum. Although certain mortar specimens

Preprints (www.preprints.org) | NOT PEER-REVIEWED | Posted: 15 June 2023 doi:10.20944/preprints202306.1135.v1

exposed to vacuum exhibited higher strength compared to those cured with water, the research concluded that vacuum conditions accelerated water loss. Concerning the development of some rover-type and robotic applications Table 13 gives some features about Moon and Mars and nearby Earth-analog exoplanets.

Table 13. Key differences between Earth, Moon, Mars and other exoplanets [14].

Parameter	Earth	Moon	Mars	Kepler-	Parameter
Total Mass Compared to Earth (%)	-	1.2	10.7	190	80-110
Approximate Distance from Earth (km)	-	$3.84x10^5$	$2.25x10^8$	$1.32x10^{16}$	$3.9x10^{13}$
Day Period (hrs)	23.9	655.7	24.7	-	-
Revolution Period (days)	365.3	27.3	686.9	384.8	11.2
Average Surface Temperature (°C)	13	-30	-57	-8	-39
Atmospheric Pressure (kPa)	101.3	negligible	0.7	unknown	unknown

2.2.2. Materials for drive system units: gears, shafts, cams, guideways, bushings

2.2.2.1. Steels [15]

Steels are often used only where lighter materials cannot be specified due to the unsuitability of their mechanical, tribological or chemical properties. Only high-strength steels (ultimate tensile strength (UTS)> 1000 MPa) are usually specified for use in spacecraft mechanisms. Maraging (martensitic) steels offer a combination of very high strength, good ductility and fracture toughness and are used in applications where weight saving is of paramount importance. Precipitation-hardening steels offer a combination of good corrosion resistance and high strength. In the as-quenched condition, these materials can be relatively easily machined because the martensite is relatively soft. Quenched and tempered steels depend on their high strength, hardness and wear resistance in the formation of a metallographic phase called martensite. Martensite is brittle and must be tempered to improve its ductility and toughness for most engineering applications. The two most commonly specified quenched and tempered steels for tribological applications in spacecraft are AISI 440C and AISI 52100. These materials are almost always used for rolling elements like bearings.

The maximum continuous operating temperature of AIS-I 440C is 240°C, however, special heat treatments and compositions allow use in the range of -269 to - 315°C.

AISI 52100 will operate at up to 150°C without distortion, however, the maximum continuous operating temperature is 125°C.

AISI 52100 is used for rolling element bearings because of its high hardness and excellent wear and fatigue resistance.

17/4PH - precipitation hardening steel is widely used across a broad spectrum of industries. It combines high strength and good corrosion properties. It can be hardened between 482°C and 621°C and air-cooled thereby eliminating scaling and minimising distortion. It maintains good ductility at sub-zero temperatures. It is magnetic.

17/5PH - similar properties to 17/4. It is ferrite free and therefore has improved notch toughness and better forgeability. 15/5PH was developed as a refinement of 17 4PH.

17/7PH - similar properties to 17/4. Good mechanical properties to 480°C and superior corrosion resistance. Used for aircraft structural parts, flat and round springs and drawn, bent or formed parts.

Alloys, such as Inconel 718, are used occasionally for spacecraft tribo-components instead of steels where there is a need for a higher temperature capability.

Inconel 600 - is usually used for severely corrosive environments at elevated temperatures. This alloy exhibits outstanding resistance to stress corrosion cracking. It should be noted that Inconel 600 cannot be hardened through heat treatment methods.

Preprints (www.preprints.org) | NOT PEER-REVIEWED | Posted: 15 June 2023 doi:10.20944/preprints202306.1135.v1

Inconel 718 - is an age-hardened high-strength alloy suitable for service in the temperature range 253°C to - 725°C. Good fatigue and stress rupture properties, good corrosion resistance.

Inconel X-750 is a non-magnetic alloy that can be age hardened, commonly chosen for its favourable corrosion and oxidation resistance, as well as its high resistance to creep rupture. Initially designed for applications in gas turbines and jet engines, this alloy is also well-suited for springs due to its exceptional relaxation resistance. It maintains good strength and ductility even at extremely low temperatures, reaching as low as -253°C. Moreover, Inconel X-750 exhibits commendable resistance to stress corrosion cracking.

PE16 – is a wrought nickel alloy specifically designed to withstand high-temperature conditions. It undergoes age-hardening and possesses exceptional creep resistance.

2.2.2.2. Aluminum alloys [14], [15]

The progress of modern aviation and exploration of outer space has gone through the engineering of aluminium alloys. Directly taken from NASA technical report [23]: "Chosen for its lightweight and able to withstand the stresses that occur during ground and launch operations, aluminium has been used on Apollo spacecraft, the Skylab, the Space Shuttles, and the International Space Station."

Aluminium alloys are selected for use in spacecraft and other mechanisms because of their low density and high specific strength. The disadvantages of aluminium alloys are their low stiffness, low hardness, high thermal expansion coefficient and susceptibility to high adhesive wear and galling. In self-mating sliding contacts in vacuum aluminium alloys exhibit high and variable friction coefficients ($\mu > 0.5$). Aluminium alloys are widely used in spacecraft mechanisms but must receive surface treatments to improve their tribological properties. Most of the alloys contain varying amounts of Mg, Cu, Si and Zn as the strengthening additions. It is summarized in Table 14.

1000 series: commercially pure aluminium. These have low strength but are very ductile.

2000 series: alloy additions of copper and magnesium. High strength. These are heat treatable. Copper additions reduce corrosion resistance.

5000 series: magnesium is the main alloying element. Non-heat-treatable. Their mechanical properties are better than 1000, 3000 and 4000 series. Good corrosion resistance.

6000 series. Heat treatable. Corrosion resistance is inferior to the 5000 series but sufficient for general engineering purposes.

7000 series: specialised alloys used mainly in aerospace applications. Heat treatable. The presence of copper reduces corrosion resistance and weldability, and strength properties are superior.

Table 14. The most typical aluminium alloys [11].

Alloy Group	Wrought Alloys Major alloying elements	Alloy Group	Cast Alloys Major alloying elements
1XXX	99.00 % minimum aluminium	1XX.0	99.00 percent minimum aluminium
2XXX	Copper	2XX.0	Copper
3XXX	Manganese	3XX.0	Silicon with added copper and/or magnesium
4XXX	Silicon	4XX.0	Silicon
5XXX	Magnesium	5XX.0	Magnesium
6XXX	Magnesium and Silicon	6XX.0	Unused Series
7XXX	Zinc	7XX.0	Zinc
8XXX	Other Elements	8XX.0	Tin
9XXX	Unused Series	9XX.0	Other Elements

The main groups used in the aerospace industry are the 2XXX, 6XXX, and 7XXX (wrought) and Al-Si casting alloys. These materials are reaching high strengths after specific conditioning. Such series are age-hardenable, and they can strengthen by this process under heat treatment [24]. The mechanical properties may decrease with an increase in the temperature above 100°C. However, in general, the strength, ductility, and toughness of the Aluminum may increase in low temperatures.

 doi:10.20944/preprints202306.1135.v1

2.2.2.3. Titanium alloys [14], [15]

Titanium alloys are widely used in spacecraft mechanisms because of their relatively low density, excellent mechanical properties and high resistance to stress corrosion cracking. The main disadvantage of titanium alloys is their poor adhesive wear resistance, and surface treatments are vital to improve the tribological performance. In self-mating sliding contacts in a vacuum, titanium alloys will exhibit high and variable friction coefficients (μ >0.5). Titanium alloys of which IMI 318 and IMI 550 are listed in ESA PSS-01-701 (ESA preferred materials). Thermo-mechanical and heat treatment procedures have been devised to ensure that alloys IMI 318 and IMI 550 provide the optimum balance of mechanical properties for a wide range of applications.

2.2.2.4. Copper-based alloys [14], [15]

There has been limited use of bronzes in spacecraft mechanisms. They are used principally as leaded bronze cages in ball bearings lubricated with ion-plated lead coatings.

Phosphor bronzes contain residual phosphorus (up to 1 wt%>) which imparts high hardness. Phosphor bronzes have high wear resistance and hardness and moderately high strength. UNS C9 0700 is so widely used for gears that it is often termed gear bronze.

Aluminium bronzes have good corrosion resistance and higher fatigue limits than any other cast copper alloy and can be used at temperatures up to 400°C without significant loss of strength. They also tend to be more resistant to galling than manganese bronzes. These materials are suitable for heavy-duty service, (valve guides, bearings, screw-down nuts and slippers) and precision machinery.

Manganese bronzes have better toughness than aluminium bronzes of equivalent tensile strength and do not require heat treatment, as strength is developed by solid solution hardening. Lead may be added to lower strength grads to improve machinability but should not exceed 0.1 wt% in the higher strength alloys. Manganese bronzes are specified for applications which require high strength, hardness and resistance to mechanical shocks such as large gears, bridge turntables, gun tracks and ordnance recoil parts. Their upper-temperature limit for use is around 230°C.

High leaded, tin bronzes are used where a softer metal than phosphor bronze is required for low load, low sliding speed applications. UNS 93700 (80-10-10) is an excellent general bearing alloy, especially well-suited for applications where lubrication may be deficient, such as-bearing cages, for use in vacuum. LB9 is used extensively for cages in bearings lubricated with ion-plated lead.

Beryllium-copper alloys possess a unique combination of mechanical and physical properties, which makes them ideal for selected applications in spacecraft mechanisms. These properties include high strength and hardness, high fatigue and creep resistance and good electrical and magnetic characteristics. In self-mating sliding contacts in vacuum, Be-Cu alloys will exhibit high and variable friction coefficients (μ> 0.5). Be-Cu alloys are used for springs that apply load to sliding contacts and for reed switches (gold coated). Cu-1.8 wt% Be, 0.3 %, wt Co-Ni (CDA 170) is listed in ESA PSS-01- 701.

2.2.2.5. High-density alloys [15]

Tungsten-based alloys containing small amounts of nickel-copper binders have high densities (comparable to tungsten) and offer improved machinability compared to pure tungsten. They are used in engineering applications requiring high inertial forces eg counterweights, gyroscope rotors, balancing weights etc. They have been tested as candidate materials for impacting surfaces in space.

2.2.2.6. Polymer composites [13], [15]

The tribological and mechanical properties of a polymer can be modified by incorporating solid fillers into the matrix. Fibres (10-20wt%) are added to engineering polymers to increase their stiffness, strength and creep resistance. These fibres are typically 5-10 μm in diameter and can be continuous, milled or chopped. Fibre size and orientation have a great effect on wear resistance and or mechanical properties. Polyamide (Kevlar), glass, carbon, nylon, polyester and cotton are all commonly specified as fibre reinforcements. Asbestos was used in the past, but is now largely avoided on safety grounds. Glass fibres are harder than many metals and may cause abrasive wear. Kevlar, carbon and graphite

 doi:10.20944/preprints202306.1135.v1

fibres are used to enhance strength, stiffness and creep resistance. Like graphite lubricants, graphitic fibres have poor tribological properties in vacuum.

Carbon or glass-fibre—filled acetal and fibre-reinforced and filled PTFE (Rulon) are commonly specified for low-precision gears in spacecraft mechanisms. Duroid is a PTFE/glass: MoS2 composite which was commonly used as a cage material for ball bearings but is no longer manufactured. PGM-HT is a material of similar composition to Duroid. For some applications requiring extreme strength: (e.g. high- speed bearing cages), woven 3-dimensional cloth (glass, cotton or carbon fibre) preforms can be impregnated with phenolic or polyester resins. These materials are supplied under the trade names Orkot, Tufnol, Ferrobestos, Railko and Tenmat. Promising material concerning temperature resistance, strength and wear resistance, high energy radiation resistance, and the different grades (natural and reinforced) of PEEK.

2.2.2.7. Ceramics [14], [15]

Light engineering ceramics such as silicon nitride, silicon carbide and alumina all have high intrinsic strength and hardness. Silicon nitride has high flexural strength (greater than 1000MPa at temperatures up to 1100°C.), high stiffness, high wear resistance hardness, good oxidation and corrosion resistance, good thermal shock resistance because of the strength of the Si-N bonds and a low thermal expansion coefficient. Silicon nitride components are usually prepared by hot pressing, although the process is expensive. Only simple shapes can be produced and the surface finish of components is inferior to the best finishes attainable with steel. High precision, hot-pressed Sh3N4(for bearings) are commercially available. Silicon nitride rings are also available but have not hitherto been favoured because of concerns over thermal expansion mismatch and cracking under tensile stresses (particularly at launch). Tungsten carbide balls are also available, their properties being similar to silicon nitrides but having a higher density.

Preprints (www.preprints.org) | NOT PEER-REVIEWED | Posted: 15 June 2023 doi:10.20944/preprints202306.1135.v1

2.2.3. Summary of possible tribo-materials for space applications

The following table (Table 15) gives a summary of tribological information on moving element materials based on literature [13]–[15].

Table 15. Summary of tribological information of material of moving elements.

Material families	**For tribological applications**			
	not recommended or strongly limited	**may be proposed with surface and structural modifications**	may be suggested (some typical application)	possibly in abrasive condition
Maraging steel		+	+	+
Precipitation-hardening steel		+	?	+
Quenched and tempered steels		+	+	+
Steel alloys: Cr, Ni alloyed steel, austenitic steels, multiphase steels				?
Aluminium alloys	+	+	?	?
Titanium alloys		+	?	?
Phosphor bronzes			+	?
Aluminium bronzes			+	?
Manganese bronzes			+	?
High-leaded tin bronzes			+	?
Beryllium-copper alloys	+			-
Tungsten-based alloy		+	?	?
Polymer Composites			+	+
Ceramics			+	?

Abrasive tested space materials published in articles [25-58] [25]–[58] are analysed and summarized in Table 16. One article may deal with two or more materials under different conditions that are taken into account in the table.

Preprints (www.preprints.org) | NOT PEER-REVIEWED | Posted: 15 June 2023 doi:10.20944/preprints202306.1135.v1

Table 16. Number of cases about materials with its conditions.

	Room conditions	Vacuum or neutral gas and room temperature	Low and high temperatures	Vacuum and high/low temperatures	With simulants
Structural steel	7	2	11	1	1
Martensitic steel	6				
Manganese steel and other alloyed steel	8		1		
Stainless steel	3	2	4		
Ceramics	11	1	1		
Rubber/elastomer	12				
Polymer/composite	3	4	1		1
Alloyed cast irons	3				
Titanium alloy	1				
WC-based sintered or hard metal	3		1		
Aluminium / coated and alloys	1	3	1	1	2

2.2.4. Identified rotary shaft and seal materials

Identified rotary shaft and seal materials (ESMATS Past Papers Database) already tested, applied and published [24], [52], [59]–[68] are concluded in Table 17.

Table 17. Shaft and seal (machine element) materials for space tested and reported.

Shaft/machine elements	Room conditions	Vacuum or neutral gas and room temperature	Low and high temperatures	Vacuum and high/low temperatures	With simulants
Aluminium	Al2024 anodized aluminium	anodized aluminium	Al2024, Al7000 series		anodized aluminium
Copper			Beryllium copper		
Steel	stainless steel	stainless steel	Nitronic 60 (stainless steel)400C, S2100		stainless steel
Titanium			Ti6Al4V		
Seal					
Polymer	PCTFE, PI/MoS_2 PTFE 3x	PTFE 3x	PCTFE, PI/MoS_2		PTFE 3x
Hybrid structure			polymer/metal		

Preprints (www.preprints.org) | NOT PEER-REVIEWED | Posted: 15 June 2023 doi:10.20944/preprints202306.1135.v1

2.2.5. Literature analyses of rotary/reciprocating shaft–seal mechanisms possibly subjected to abrasive conditions

Concerning articles on different space mechanisms [23], [52], [60], [68]–[94] are evaluated. Mechanisms, shaft materials, sealings and bearing solutions are identified. In Table 18 and Table 19, the conclusions are summarized.

Table 18. Grouping of mechanisms.

Mechanism	Number of case
any rover applications	4
open-close mechanisms	6
positioning mechanisms/mechatronics	4
berthing - docking	4
robotic arm	4
doors	4
other rotary/reciprocating shafts	5

Table 19. Shaft and seal materials identified in mechanisms.

Shaft materials	Number of cases
Cooper – beryllium alloy	4
Titanium alloy	7
Al and Al alloy	9
Stainless steel	9
Other steel alloys	4
Seal materials	Number of cases
PTFE	19
PTFE - composite	4
Hybrid: metal/polymer combinations	1
Metallic	3
Other polymers (HPM, UHMW-PE…)	6

As it is reported, stainless steel and Al versions are commonly applied materials as shaft materials, while seal solutions are preferred of PTFE natural or other grades even with metallic combinations. The reported cases mainly belong to the low-speed sliding mechanism, where the sliding speed can vary between 0 – 0.1 -0.2 m/s, with both roller (ball) and slide bearing solutions.

3. Review on application of Martian and Lunar simulants.

Several application examples are to be considered for the selection of simulants. For instance, on Mars, layers of dust accumulate on solar panels due to atmospheric transport, diminishing their efficiency. Additionally, dust storms disperse particles across exposed surfaces. On the Moon, the lack of atmosphere prevents the transportation of particles by winds. However, various activities such as firing descent thrusters, rover wheel movements, solar charging, and instrument interactions with lunar regolith can stir up dust and contaminate surfaces. T. Tattusch et al [95] observed a variety of effects contingent upon the celestial body on which a space system operates. For the ESA DEAR (Dusty Environment & Robotics) project, a special test bench was set up to perform environmental tests. Four different simulants have been applied. ISO reference dust eskal 60, ISO reference dust eskal 150, Lunar Regolith Simulant TUBS-T and Lunar Regolith Simulant TUBS-M. The advantages of ISO simulants were non-hygroscopic behaviour and simple handling and storage, while the drawback was different particle size distributions from the real samples. TUBS lunar regolith simulants were very similar to real lunar samples in chemistry, particle size distribution and particle shape. However, sharp-edged fine dust required special safety instructions and precautions.

Preprints (www.preprints.org) | NOT PEER-REVIEWED | Posted: 15 June 2023 doi:10.20944/preprints202306.1135.v1

Budzyn et al [96] performed topology optimization as a design method to enhance hardware performance in the Lunar dust environment. The knowledge gained from the Apollo missions revealed that Lunar regolith particles possess sharp edges, carry electrostatic charges, exhibit adhesive properties, and pose a significant risk to mission hardware. They can infiltrate gaps between mechanical elements and cause damage, particularly in scenarios involving rigid body relative displacements. In this context, an alternative design strategy for Lunar surface hardware is proposed. The authors suggest utilizing compliant mechanisms to create monolithic structures that inherently withstand Lunar dust effects. To facilitate the design of compliant mechanisms topology-optimization based design methods are to be adopted. Topology optimization aims to optimize material distribution for a given design space and boundary conditions to maximize the performance of the design. The study explores several MATLAB routines that can assist in topology optimization for compliant mechanisms. Each routine's advantages and disadvantages are outlined, and their application to a compliant force inverter is demonstrated.

During the preliminary assessment of seals for dust mitigation in mechanical components for Martian and Lunar surface systems, various factors were taken into account by E.T. Baumgartner [97] as well as Harrington et al [98]. To evaluate the effectiveness of spring-loaded Teflon seals in preventing lunar simulant from entering gearbox, motor, and bearing housings of mechanical components, component tests were conducted. Baseline tests were performed in a dry room without simulant over 10,000 cycles to assess seal wear against anodized aluminum or stainless steel shafts. Subsequent tests were conducted using lunar simulants JSC-1A and LHT-2M. Additionally, tests were conducted under vacuum conditions at ambient temperature, both with and without the presence of simulant. Preliminary findings indicate minimal wear on the seals and shafts after 10,000 cycles. Most importantly, no simulant was observed to pass through the seal-shaft interface. To further evaluate endurance, future tests are planned using NASA Lunar Surface System architecture shaft sizes and relevant operating conditions.

4. Discussion and conclusion

Based on the available simulants, chemical/physical properties and application use cases, a decision was made about technical selection criteria for our tribological testing.

Additional, non-technical selection criteria have been considered. Preparation of certain simulants requires a costly and long process and results in a small amount of simulants. Selection criteria were introduced to reflect the delivery lead time and cost of simulant /kg. Considering our technical review results, the mineralogical form and particle shape of the simulant are more important than the pure chemical substance ratio. Simulants to be selected, that represent more the landing site and are as similar as reasonably possible to the real soil samples. It is preferred to have high mineralogical fidelity, but consider limitations due to Earth-based component sourcing.

According to these two criteria, and considering the contradiction of using Earth-based raw material to prepare Moon and Mars simulants, the core selection requirements are:

- Level of mineralogical fidelity: particle shape and form relevant to abrasion test allowing for good representativity of the test with real Lunar/Martian regolith
- Particle size distribution
- Density and gravity
- Information basis of the preparation of simulants

The following tables (Table 20 and Table 21) are mapping the simulants and the criteria described above.

Preprints (www.preprints.org) | NOT PEER-REVIEWED | Posted: 15 June 2023 doi:10.20944/preprints202306.1135.v1

Table 20. Comparison of Lunar simulants based on Mineralogical fidelity, price and availability.

Simulant type	Name	Supplier	Country	Description	Particle size range	Mineralogical fidelity	Price	Availability
Lunar Mare	LMS-1	Exolith Lab	USA	High mineralogical fidelity	<0.04 µm – 300 µm		$35/kg	Available
	OPRL2N	Off Planet Research	USA	Mechanical simulant	Apollo 17 PSD		About $80/kg	Available
	UoM-B & UoM-W	University of Manchester	UK	Low-fidelity, angular grain shapes	B: 0.1 - 0.7mm W: < 125µm			From feedstock supplier
	TUBS-M	TU Braunschweig	Germany	ISRU-oriented base simulant, customizable	0 – 2 mm			
Lunar Highland	LHS-1	Exolith Lab	USA	High mineralogical fidelity, Sub angular grains, lower specific gravity	<0.04 µm – 400 µm		$35/kg	Available
	Greenspar	Hudson Resources	Greenland	High anorthite content	<250 µm or <90 µm	High An%	Unknown	Available
	OPRH2N	Off Planet Research	USA	Mechanical simulant	Apollo highland sample PSD average	High An%	About $80/kg	Available
	OB-1	Deltion Innovations	Canada	High glass content, angular grains, high specific gravity	Apollo 16 sample 64500 PSD	High An%	Unknown	Unknown
	TUBS-T	TU Braunschweig	Germany	ISRU-oriented base simulant, customizable	0 – 2 mm	Customizable		

Colour coding means the following.

Mineralogical fidelity (compared with their respective reference material):
Red: Low
Yellow: Moderate fidelity
Green: High

Preprints (www.preprints.org) | NOT PEER-REVIEWED | Posted: 15 June 2023 doi:10.20944/preprints202306.1135.v1

Price of 5kg simulant (product only):
Red: Over EUR500
Yellow: Unknown
Green: Less than EUR500

Availability (5kg or more):
Red: Not available
Yellow: Unknown
Green: Available for acquisition

Lead Time (from order placement to ready for shipment):
Red: Longer than 2 months or not available
Yellow: Between 1- 2 months, or unknown
Green: Within 1 month

Table 21. Comparison of Martian simulants based on Mineralogical fidelity, price and availability.

Simulant type	Name	Supplier	Country	Description	Particle size range	Mineralogical fidelity	Price	Availability
Mars	MGS-1	Exolith Lab	USA	High mineral, chemical, volatile and spectral fidelities	>0.04 µm – 600 µm		$35/kg	Available
	ES-x	Varies	Europe	Geotechnical simulants in different size ranges	1: < 10 – 32µm 2: ~ >30 – 125 µm 3: ~ >30 – 20,000 µm 4: ~ 0.1 – 500 µm			Some available from ESA or supplier
	OUCM OUEB OUHR OUSR	Open University	UK	Astrobiology simulants. Each has a standard composition (-1) and adjusted Fe^{2+} concentration (-2).	200 – 2000 µm			

Preprints (www.preprints.org) | NOT PEER-REVIEWED | Posted: 15 June 2023 doi:10.20944/preprints202306.1135.v1

	JSC Mars-1	NASA JSC	USA	Spectral analogue, supports general scientific and engineering studies	< 1 mm		Only pay for shipping	Available
	P/S-MRS	DLR	Germany	For Raman spectral studies	< 1 mm		Unknown	Unknown
Mars Jezero	JEZ-1	Exolith Lab	USA	MGS-1 mixed with smectite, Mg-carbonate, and additional olivine	< 0.04 - 500 µm		$35/kg	Available

Colour coding means the following.

Mineralogical fidelity (compared with their respective reference material):
Red: Low
Yellow: Moderate fidelity
Green: High

Price of 5kg simulant (product only):
Red: Over EUR500
Yellow: Unknown
Green: Less than EUR500

Availability (5kg or more):
Red: Not available
Yellow: Unknown
Green: Available for acquisition

Lead Time (from order placement to ready for shipment):
Red: Longer than 2 months or not available
Yellow: Between 1- 2 months, or unknown
Green: Within 1 month

Preprints (www.preprints.org) | NOT PEER-REVIEWED | Posted: 15 June 2023 doi:10.20944/preprints202306.1135.v1

Considering the options listed in Table 20 and Table 21, four different simulants have been identified for our purpose.

LMS-1: The first sample aims to represent a generic or average mare location on the Moon. It is a highly accurate mineral-based simulant specifically tailored for this purpose. Instead of being composed of a single terrestrial lithology, it successfully replicates the lunar regolith's texture by combining mineral and rock fragments (polymineralic grains) in precise proportions. The simulant's particle size distribution is designed to match that of typical Apollo soils.

LHS-1: The second sample is designed to simulate Lunar Highlands. It is a mineral-based simulant suitable for a generic or average highlands location on the Moon. Like the previous simulant, it does not consist of a single terrestrial lithology. However, it accurately captures the texture of lunar regolith. The particle size distribution of this simulant is carefully adjusted to resemble that of typical Apollo soils.

MGS-1: The third sample aims to represent Mars. It serves as a mineralogical standard for basaltic soils found on Mars, developed based on quantitative mineralogy obtained from the MSL Curiosity rover. Specifically, it seeks to replicate the composition of the Rocknest windblown soil, which chemically resembles other basaltic soils at various landing sites, making it a suitable "global" basaltic soil representation. The development process involves sourcing individual minerals, including appropriate treatment of the X-ray amorphous component.

JEZ-1: The fourth sample is designed to mimic the anticipated materials found in the Jezero Crater deltas, which are being investigated by the NASA Mars 2020 rover. This simulant is a blend of the previous sample (Sample 3 – MGS-1) with smectite clay, Mg-carbonate, and additional olivine. The selection of these components is based on their detection through orbital remote sensing in the Jezero delta deposits.

Figure 2. shows the selected soil simulants.

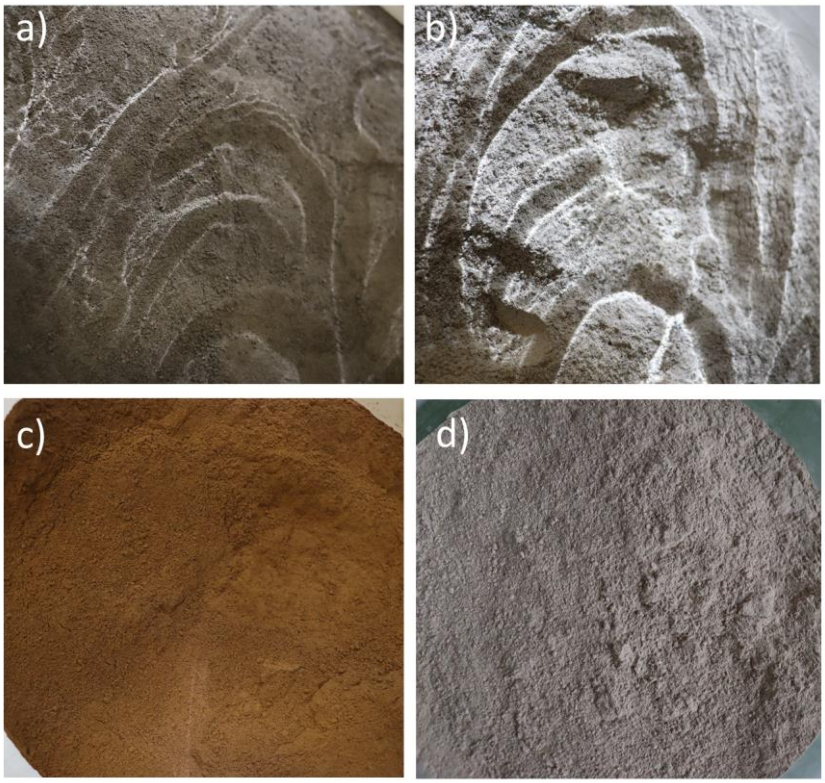

Figure 2. Selected soil simulants: a) LMS-1 lunar mare, b) LHS-1 lunar highland, c) MGS-1 Mars general, d) JEZ-1 Mars Jezero.

Concerning the structural materials of shaft solutions paired with any kind of sealings against abrasive particles, the following order can be seen based on numerous published case studies and

Preprints (www.preprints.org) | NOT PEER-REVIEWED | Posted: 15 June 2023 doi:10.20944/preprints202306.1135.v1

research reports (the most frequent published materials at the beginning of the list, the less frequent ones at the end):

- structural and martensitic- and manganese steel grades
- stainless steel grades
- high-strength aluminium, anodized
- other aluminium alloys
- polymer/composites
- ceramics
- Ti alloys

The following structural materials were selected for the further detailed study of the abrasion effect and the research of a sealed rotating shaft subjected to simulant particles:

- rotary shaft materials: stainless steel 1.4404 and hard anodized Al 7075 (Figure 3)
- sealing materials: natural PTFE and a composite PTFE/15%GF+5%MoS_2 lipseals and packings (Figure 4)

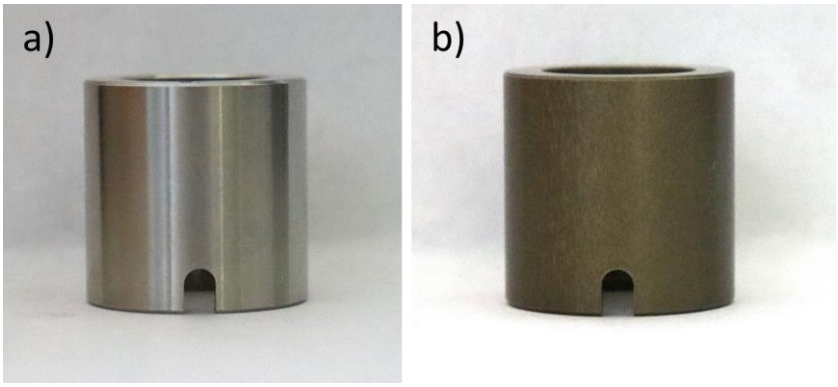

Figure 3. a) Stainless steel and b) Anodized Al shaft samples for further research.

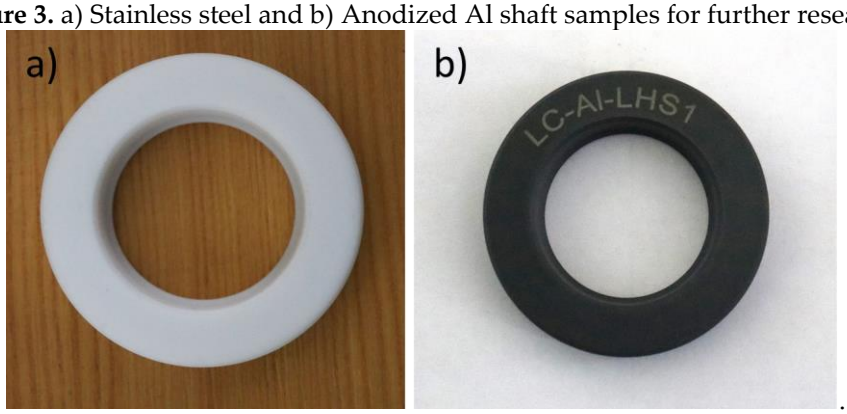

Figure 4. a) Natural and b) composite PTFE lipseal samples.

Author Contributions: Conceptualization: Gy.B. and G.K.; writing—original draft preparation: Á.K., H.S., Gy.B. and G.K; writing—review and editing: Á.K and B.Gy; visualization: R.K and L.Zs.; supervision and project administration: Gy.B. and G.K.

Funding: This research was funded by ESA, Contract No. 4000136800/21/NL/CBi

Acknowledgments: Authors express special thanks to Kamini Manick, SACF Curator and Laboratory Coordinator and Xiao Chen Zhang, SACF Young Graduate Trainee for their contribution to the data collection, and support of the analysis. The authors would like to acknowledge the support of Ewelina Ryszawa. Special thanks to Dr. Linke, Stefan and Joel James Patzwald, Technische Universität Berlin, for the TUBS-T and TUBS-M simulant samples.

Conflicts of Interest: The authors declare no conflict of interest.

References

[1] T. P. Gouache *et al.*, "Soil simulant sourcing for the ExoMars rover testbed," *Planetary and Space Science*, vol. 59, no. 8, pp. 779–787, Jun. 2011, doi: 10.1016/j.pss.2011.03.006.

[2] M. Alexander, "Mars transportation environment definition document," *NASA Technical Memorandum*, no. 210935, 2001, Accessed: Jun. 07, 2023. [Online]. Available: http://www.sti.nasa.gov.

[3] T. Newson, A. Ahmed, D. Joshi, X. Zhang, and G. R. Osinski, "Assessment of the Geomechanical Properties of Lunar Simulant Soils," in *Earth and Space 2021: Space Exploration, Utilization, Engineering, and Construction in Extreme Environments - Selected Papers from the 17th Biennial International Conference on Engineering, Science, Construction, and Operations in Challenging Environments*, 2021, pp. 146–156, doi: 10.1061/9780784483374.015.

[4] U. Böttger, J. P. De Vera, J. Fritz, I. Weber, H. W. Hübers, and D. Schulze-Makuch, "Optimizing the detection of carotene in cyanobacteria in a martian regolith analogue with a Raman spectrometer for the ExoMars mission," in *Planetary and Space Science*, Jan. 2012, vol. 60, no. 1, pp. 356–362, doi: 10.1016/j.pss.2011.10.017.

[5] C. C. Allen, R. V. Morris, M. J. Karen, D. C. Golden, M. M. Lindstrom, and J. P. Lockwood, "Martian regolith simulant JSC Mars-1," in *Lunar and planetary science conference XXIX*, 1998, no. Table 2, p. 1690, Accessed: Jun. 07, 2023. [Online]. Available: https://ui.adsabs.harvard.edu/abs/1998LPI....29.1690A/abstract.

[6] K. M. Cannon, D. T. Britt, T. M. Smith, R. F. Fritsche, and D. Batcheldor, "Mars global simulant MGS-1: A Rocknest-based open standard for basaltic martian regolith simulants," *Icarus*, vol. 317, pp. 470–478, Jan. 2019, doi: 10.1016/j.icarus.2018.08.019.

[7] G. H. Just, K. H. Joy, M. J. Roy, and K. L. Smith, "Geotechnical characterisation of two new low-fidelity lunar regolith analogues (UoM-B and UoM-W) for use in large-scale engineering experiments," *Acta Astronautica*, vol. 173, pp. 414–424, Aug. 2020, doi: 10.1016/j.actaastro.2020.04.025.

[8] S. Linke *et al.*, "TUBS-M and TUBS-T based modular Regolith Simulant System for the support of lunar ISRU activities," *Planetary and Space Science*, vol. 180, p. 104747, Jan. 2020, doi: 10.1016/j.pss.2019.104747.

[9] "https://www.offplanetresearch.com/simulants-feedstocks-and-additives." .

[10] "https://exolithsimulants.com/collections/regolith-simulants/products/lms-1-lunar-mare-simulant." .

[11] J. Gruener, J. E.; Deitrick, S. R.; Tu, V. M.; Clark, J. V.; Ming, D. W.; Cambon, "Greenland 'White Mountain' Anorthosite: A new Lunar polar regolith simulant component," 2020. https://hudsonresource-sinc.com/nasa-greenspar-lunar-simulant-abstract-greenland-white-mountain-anorthosite-a-new-lunar-polar-regolith-simulant-component/ (accessed Jun. 07, 2023).

[12] M. M. Battler and J. G. Spray, "The Shawmere anorthosite and OB-1 as lunar highland regolith simulants," *Planetary and Space Science*, vol. 57, no. 14–15, pp. 2128–2131, Dec. 2009, doi: 10.1016/j.pss.2009.09.003.

[13] J. Chen, N. Ding, Z. Li, and W. Wang, "Organic polymer materials in the space environment," *Progress in Aerospace Sciences*, vol. 83. Pergamon, pp. 37–56, May 01, 2016, doi: 10.1016/j.paerosci.2016.02.002.

[14] M. Z. Naser and A. I. Chehab, "Materials and design concepts for space-resilient structures," *Progress in Aerospace Sciences*, vol. 98. Pergamon, pp. 74–90, Apr. 01, 2018, doi: 10.1016/j.paerosci.2018.03.004.

[15] E. W. Roberts and M. Eiden, *A Space Tribology Handbook*. Warrington: European Space Tribology Laboratory, 2013.

[16] S. Lim and M. Anand, "Space Architecture technology for settlement and exploration on other planetary bodies – In-Situ Resource Utilisation (ISRU) based structures on the Moon," May 2014, Accessed: Jun. 07, 2023. [Online]. Available: https://els2014.arc.nasa.gov.

[17] "Mars' atmosphere: Facts about the composition and climate." https://www.space.com/16903-mars-atmosphere-climate-weather.html (accessed Mar. 18, 2022).

[18] N. J. Lindsey, "Lunar Station Protection: Lunar Regolith Shielding," *International Lunar Conference*, p. 143, 2004.

[19] H. A. Toutanji, S. Evans, and R. N. Grugel, "Performance of lunar sulfur concrete in lunar environments," *Construction and Building Materials*, vol. 29, pp. 444–448, Apr. 2012, doi: 10.1016/J.CONBUILDMAT.2011.10.041.

[20] J. Nealy, J. Wilson, and L. Townsend, "Solar-flare shielding with Regolith at a lunar-base site," *NASA Technical Paper*, 1989.

[21] H. Kanamori, S. Matsumoto, and N. Ishikawa, "Long-term properties of mortar exposed to a vacuum," in *American Concrete Institute, ACI Special Publication*, May 1991, vol. SP-125, pp. 57–69, doi: 10.14359/2415.

[22] J. A. Duffie and W. A. Beckman, *Solar Engineering of Thermal Processes*, 4th ed. Solar Energy Laboratory University of Wisconsin-Madison, 2013.

[23] E. Uythoven, P.-A. Mäusli, C. Toussaint, M. Udriot, and J.-P. Kneib, "Design of a novel separation mechanism for high-power model rockets," 2021.

[24] S. Kanji and M. Buratynsky, "Challenges Associated With Testing Mechanisms for a Martian Environement," 2019.

[25] J. J. Penagos, J. I. Pereira, P. C. Machado, E. Albertin, and A. Sinatora, "Synergetic effect of niobium and molybdenum on abrasion resistance of high chromium cast irons," *Wear*, vol. 376–377, pp. 983–992, Apr. 2017, doi: 10.1016/j.wear.2017.01.103.

[26] J. Qiu *et al.*, "Effects of niobium particles on the wear behavior of powder metallurgical γ-TiAl alloy in different environments," *Wear*, vol. 434–435, p. 202964, Sep. 2019, doi: 10.1016/J.WEAR.2019.202964.
[27] R. Dalai, S. Das, and K. Das, "Effect of thermo-mechanical processing on the low impact abrasion and low stress sliding wear resistance of austenitic high manganese steels," *Wear*, vol. 420–421, pp. 176–183, Feb. 2019, doi: 10.1016/J.WEAR.2018.10.013.
[28] J. N. Mpagazehe, K. W. Street, I. R. Delgado, and C. Fred Higgs, "An experimental study of lunar dust erosive wear potential using the JSC-1AF lunar dust simulant," *Wear*, vol. 316, no. 1–2, pp. 79–91, Aug. 2014, doi: 10.1016/J.WEAR.2014.04.018.
[29] C. A. Bühler, "Experimental investigation of lunar dust impact wear," *Wear*, vol. 342–343, pp. 244–251, Nov. 2015, doi: 10.1016/J.WEAR.2015.09.002.
[30] A. Sengupta, J. Kulleck, J. Van Norman, and M. Mehta, "Thermal coating erosion in a simulated Martian landing environment," *Wear*, vol. 270, no. 5–6, pp. 335–343, Feb. 2011, doi: 10.1016/J.WEAR.2010.09.013.
[31] Z. Pei, R. Song, Q. Ba, and Y. Feng, "Dimensionality wear analysis: Three-body impact abrasive wear behavior of a martensitic steel in comparison with Mn13Cr2," *Wear*, vol. 414–415, pp. 341–351, Nov. 2018, doi: 10.1016/J.WEAR.2018.09.002.
[32] L. Huang, X. Deng, C. Li, Y. Jia, Q. Wang, and Z. Wang, "Effect of TiC particles on three-body abrasive wear behaviour of low alloy abrasion-resistant steel," *Wear*, vol. 434–435, p. 202971, Sep. 2019, doi: 10.1016/J.WEAR.2019.202971.
[33] Y. Li and Y. Gao, "Three-body abrasive wear behavior of CC/high-Cr WCI composite and its interfacial characteristics," *Wear*, vol. 268, no. 3–4, pp. 511–518, Feb. 2010, doi: 10.1016/J.WEAR.2009.09.001.
[34] A. P. Harsha, "An investigation on low stress abrasive wear characteristics of high performance engineering thermoplastic polymers," *Wear*, vol. 271, no. 5–6, pp. 942–951, Jun. 2011, doi: 10.1016/J.WEAR.2011.03.019.
[35] L. Huang, X. Deng, Y. Jia, C. Li, and Z. Wang, "Effects of using (Ti,Mo)C particles to reduce the three-body abrasive wear of a low alloy steel," *Wear*, vol. 410–411, pp. 119–126, Sep. 2018, doi: 10.1016/J.WEAR.2018.06.008.
[36] C. Y. Hu *et al.*, "On the impacts of grain refinement and strain-induced deformation on three-body abrasive wear responses of 18Cr–8Ni austenitic stainless steel," *Wear*, vol. 446–447, p. 203181, Apr. 2020, doi: 10.1016/J.WEAR.2019.203181.
[37] M. Varga, "High temperature abrasive wear of metallic materials," *Wear*, vol. 376–377, pp. 443–451, Apr. 2017, doi: 10.1016/J.WEAR.2016.12.042.
[38] J. J. Penagos, F. Ono, E. Albertin, and A. Sinatora, "Structure refinement effect on two and three-body abrasion resistance of high chromium cast irons," *Wear*, vol. 340–341, pp. 19–24, Oct. 2015, doi: 10.1016/J.WEAR.2015.03.020.
[39] M. Antonov, I. Hussainova, R. Veinthal, and J. Pirso, "Effect of temperature and load on three-body abrasion of cermets and steel," *Tribology International*, vol. 46, no. 1, pp. 261–268, Feb. 2012, doi: 10.1016/J.TRIBOINT.2011.06.029.
[40] M. Shah and S. Das Bakshi, "Three-body abrasive wear of carbide-free bainite, martensite and bainite-martensite structure of similar hardness," *Wear*, vol. 402–403, pp. 207–215, May 2018, doi: 10.1016/J.WEAR.2018.02.020.
[41] M. Varga, H. Rojacz, H. Winkelmann, H. Mayer, and E. Badisch, "Wear reducing effects and temperature dependence of tribolayer formation in harsh environment," *Tribology International*, vol. 65, pp. 190–199, Sep. 2013, doi: 10.1016/J.TRIBOINT.2013.03.003.
[42] S. Das Bakshi, D. Sinha, S. Ghosh Chowdhury, and V. V. Mahashabde, "Surface and sub-surface damage of 0.20 wt% C-martensite during three-body abrasion," *Wear*, vol. 394–395, pp. 217–227, Jan. 2018, doi: 10.1016/J.WEAR.2017.07.004.
[43] P. Mukhopadhyay, P. S. Kannaki, M. Srinivas, and M. Roy, "Microstructural developments during abrasion of M50 bearing steel," *Wear*, vol. 315, no. 1–2, pp. 31–37, Jul. 2014, doi: 10.1016/J.WEAR.2014.03.010.
[44] S. M. Nahvi, P. H. Shipway, and D. G. McCartney, "Particle motion and modes of wear in the dry sand–rubber wheel abrasion test," *Wear*, vol. 267, no. 11, pp. 2083–2091, Oct. 2009, doi: 10.1016/J.WEAR.2009.08.013.
[45] M. Jokari-Sheshdeh, Y. Ali, S. C. Gallo, W. Lin, and J. D. Gates, "Comparing the abrasion performance of NiHard-4 and high-Cr-Mo white cast irons: The effects of chemical composition and microstructure," *Wear*, vol. 492–493, p. 204208, Mar. 2022, doi: 10.1016/J.WEAR.2021.204208.
[46] H. Ramadas, S. Sarkar, and A. K. Nath, "Three-body dry abrasive wear properties of 15–5 precipitation hardening stainless steel produced by laser powder bed fusion process," *Wear*, vol. 470–471, p. 203623, Apr. 2021, doi: 10.1016/J.WEAR.2021.203623.
[47] C. A. Damião, G. C. Alcarria, V. C. Teles, J. D. B. de Mello, and W. M. da Silva, "Influence of metallurgical texture on the abrasive wear of hot-rolled wear resistant carbon steels," *Wear*, vol. 426–427, pp. 101–111, Apr. 2019, doi: 10.1016/J.WEAR.2019.01.046.

[48] S. Zafar and A. K. Sharma, "Abrasive and erosive wear behaviour of nanometric WC–12Co microwave clads," *Wear*, vol. 346–347, pp. 29–45, Jan. 2016, doi: 10.1016/J.WEAR.2015.11.003.
[49] Y. Jian, Z. Huang, J. Xing, and J. Li, "Effects of chromium additions on the three-body abrasive wear behavior of Fe-3.0 wt% B alloy," *Wear*, vol. 378–379, pp. 165–173, May 2017, doi: 10.1016/J.WEAR.2017.02.042.
[50] S. Hernandez, J. Hardell, H. Winkelmann, M. R. Ripoll, and B. Prakash, "Influence of temperature on abrasive wear of boron steel and hot forming tool steels," *Wear*, vol. 338–339, pp. 27–35, Sep. 2015, doi: 10.1016/J.WEAR.2015.05.010.
[51] M. Petrica, C. Katsich, E. Badisch, and F. Kremsner, "Study of abrasive wear phenomena in dry and slurry 3-body conditions," *Tribology International*, vol. 64, pp. 196–203, Aug. 2013, doi: 10.1016/J.TRIBOINT.2013.03.028.
[52] I. R. Delgado and M. J. Handschuh, "Preliminary Assessment of Seals for Dust Mitigation of Mechanical Components for Lunar Surface Systems," *NASA/CP-2010-216272*, 2010.
[53] K. G. Budinski, "Adhesive transfer to abrasive particles in abrasion testing," *Wear*, vol. 271, no. 9–10, pp. 1258–1263, Jul. 2011, doi: 10.1016/J.WEAR.2010.11.036.
[54] J. M. Fildes, S. J. Meyers, C. P. Mulligan, and R. Kilaparti, "Evaluation of the wear and abrasion resistance of hard coatings by ball-on-three-disk test methods—A case study," *Wear*, vol. 302, no. 1–2, pp. 1040–1049, Apr. 2013, doi: 10.1016/J.WEAR.2012.11.018.
[55] M. R. Thakare, J. A. Wharton, R. J. K. Wood, and C. Menger, "Effect of abrasive particle size and the influence of microstructure on the wear mechanisms in wear-resistant materials," *Wear*, vol. 276–277, pp. 16–28, Feb. 2012, doi: 10.1016/J.WEAR.2011.11.008.
[56] A. Nieto, H. Yang, L. Jiang, and J. M. Schoenung, "Reinforcement size effects on the abrasive wear of boron carbide reinforced aluminum composites," *Wear*, vol. 390–391, pp. 228–235, Nov. 2017, doi: 10.1016/J.WEAR.2017.08.002.
[57] M. Woldman, E. van der Heide, D. J. Schipper, T. Tinga, and M. A. Masen, "Investigating the influence of sand particle properties on abrasive wear behaviour," *Wear*, vol. 294–295, pp. 419–426, Jul. 2012, doi: 10.1016/J.WEAR.2012.07.017.
[58] K. Qin *et al.*, "Non-uniform abrasive particle size effects on friction characteristics of FKM O-ring seals under three-body abrasion," *Tribology International*, vol. 136, pp. 216–223, Aug. 2019, doi: 10.1016/J.TRIBOINT.2019.03.051.
[59] D. Grandy, N. Panek, G. Routhier, and P. Ridolfi, "Development And Qualification Of The Exomars Bogie Electro-Mechanical Assembly (Bema) Rotary Actuators," 2019.
[60] S. Dougherty, "Micro-imager dust cover, micro-imager contact sensor, and mössbauer spectrometer contact sensor mechanisms for the mars exploration rovers," in *European Space Agency, (Special Publication) ESA SP*, 2003, vol. 524, no. 524, pp. 73–80, Accessed: Jun. 08, 2023. [Online]. Available: https://ui.adsabs.harvard.edu/abs/2003ESASP.524...73D/abstract.
[61] L. Jandura, "Mars Science Laboratory Sample Acquisition, Sample Processing and Handling: Subsystem Design and Test Challenges," *Proceedings of the 40th Aerospace Mechanisms Symposium*, 2010.
[62] T. C. Ng and K. L. Yung, "Mars Rock Corer and Planetary Micro Sampling Tools," *Proceedings of the 33rd Lunar and Planetary Science Conference*, 2010.
[63] B. Arkwright, P. Buchele, and P. Di Leonardo, "Development of a modular two-axis gimbal mechanism for spacecraft antenna and thruster pointing," 1999.
[64] description of harmonic gear assembly operation Harmonic Drive LLC web site, "http://harmonicdrive.com/." .
[65] M. McClendon, "NIRSpec MSS Magnet Actuator Life Test Unit Wear Particle Evaluation," 2011.
[66] J. Galary, "Rolling Wear and Fatigue in Lubricated Contacts," University of Massachusetts at Dartmouth, 2018.
[67] E. Lamotte, J.-L. Bozet, and A. Kabuya, "Modelling of friction and wear for cryogenic valve seals of rocket engines," *Techspace Aero*, 2000.
[68] B. Provedo, G. Jaio, and J. Viñals, "Sealing cap for metis instrument in solar orbiter fdm subsystem," in *ESMATS 2017*, 2017, no. September, pp. 20–22.
[69] M. Sidz, Ł. Powęska, N. Wilson, and S. Pulker, "Umbilical Release Mechanisms (URM) for exomars2020 mission," *European Space Mechanisms and Tribology Symposium 2019*, no. September, pp. 18–20, 2019.
[70] F. Fouché, F. Leproux, M. Leverd, and J. Sicre, "Development and qualification of a High-Temperature Shape Memory Alloys based Actuator for Hold Down and Release Mechanisms (HDRM)," 2021.
[71] Ł. Powęska, M. Sidz, and G. Ybarra, "Qualification of resource transfer mechanisms as part of international berthing and docking mechanism – hard capture system development," 2021.
[72] S. Obara, A. Sasaki, M. Haraguchi, K. Imagawa, M. Nishimura, and N. Kawashima, "Evaluation tests of industrial vacuum bearings for space use," 2001.
[73] M. Schmalbach, M. Eigenmann, and T. Schmidt, "Development of a two hinge shutter and calibration mechanism," 2011, Accessed: Jun. 08, 2023. [Online]. Available: www.enmap.com.
[74] D. Verhoeven and D. Renté, "Locking mechanism for ixv re-entry demonstrator flap control system," 2011.

[75] J. Viñals, C. Borque, G. Jaio, and B. Provedo, "Doors mechanism for feedthrough operation in solar orbiter FDM subsystem," *16th European Space Mechanisms and Tribology Symposium 2015*, 2015.
[76] M. Garland *et al.*, "Design and implementation of the Lightweight Advanced Robotic Arm Demonstrator (LARAD)," 2017.
[77] B. Strube *et al.*, "Exomars Pancam High Resolution Camera (HRC): evolution from BB to FM," 2019.
[78] W. R. Jones *et al.*, "The tribological properties of several silahydrocarbons for use in space mechanisms," 2001.
[79] L. Cadiergues *et al.*, "A mirror control mechanism for space telescope," 2003.
[80] S. Henein *et al.*, "Mechanical slit mask mechanism for the james webb space telescope spectrometer," 2003.
[81] G. C. Caprini *et al.*, "Main port mechanism for prisma," 2013.
[82] T. Mohtar, A. Bursi, A. Galbiati, and M. Spinelli, "Actuated cover door with emergency opening function for space telescopes," 2021.
[83] N. Nava, M. Collado, and R. Cabás, "New deployment mechanisms based on sma technology for space applications," 2013.
[84] M. Thiel *et al.*, "The Rosetta lander anchoring system," 2003.
[85] R. Billing, "Caging mechanisms for the mars exploration rover instrument deployment device," 2003, Accessed: Jun. 08, 2023. [Online]. Available: http://www.asi-space.com.
[86] P. Author Rius Billing and C.-A. Richard Fleischner, "Mars science laboratory robotic arm," 2011.
[87] E. Urgoiti, A. Ramirez, and P. Coste, "GAIA M2M positioning mechanism," 2005.
[88] P. Campo, A. Barrio, N. Puente, and R. Kyle, "Development of a high temperature antenna pointing mechanisms for bepicolombo planetary orbiter," 2013.
[89] M. Gewehr, A. Schneider, J. Dalcolmo, S. Klinkner, and S. Gmbh, "Design and testing of a novel miniaturised sealed tether-recoil mechanism for the nanokhod microrover," *ESMATS-2021*, no. 1, 2021.
[90] B. Schmid, P. Flüeli, P. Houghton, and D. Blum, "Development of the lid opening mechanism (LOM)," *13th European Space Mechanisms & Tribology Symposium*, 2009.
[91] C. Melzer, A. Alegre Cubillo, M. Nadler, F. Pfitzner, and R. Hahn, "Mechanical Testing on the Core Sample Transportation Mechanism of the ExoMars 2018 Mission," in *ESA Special Publication*, Sep. 2015, vol. 737, p. 53.
[92] R. Paul *et al.*, "'Backlash-free' gas-tight high precision sample handling mechanisms – lessons learned from qualification testing & Design and lessons learned of the core sample handling mechanism (cshs) on the Exomars 2020 rover," 2017.
[93] E. Suetta *et al.*, "Four cover mechanisms for the Rosetta mission," *ESASP*, vol. 438, p. 127, 1999, Accessed: Jun. 08, 2023. [Online]. Available: https://ui.adsabs.harvard.edu/abs/1999ESASP.438..127S/abstract.
[94] L. Kiener, G. Perruchoud, P. Schwab, A. Verhaeghe, P. Spanoudakis, and M. Gumy, "Development challenges of a focus mechanism for EXOMARS mission submitted to the harsh Martian environment," in *ESMATS 2017*, 2018, p. 39, doi: 10.1117/12.2311976.
[95] T. Tattusch *et al.*, "DEAR-Providing a dusty environment for planetary exploration robotics testing," 2021.
[96] D. Budzyn, H. Zare-Behtash, A. Cowley, and A. Cammarano, "Topology optimization of compliant mechanisms as a design method to improve hardware performance in lunar dust environment," 2021.
[97] E. T. Baumgartner, R. G. Bonitz, J. P. Melko, L. R. Shiraishi, and P. C. Leger, "The Mars Exploration Rover instrument positioning system," *2005 IEEE Aerospace Conference*, 2005, Accessed: Jun. 07, 2023. [Online]. Available: https://www.academia.edu/4453248/The_Mars_Exploration_Rover_instrument_positioning_system.
[98] B. D. Harrington and C. Voorhees, "The Challenges of Designing the Rocker-Bogie Suspension for the Mars Exploration Rover," *37th Aerospace Mechanisms Symposium*, 2004.